

Kinetic dissipation and anisotropic heating in a turbulent collisionless plasma

T. N. Parashar, M. A. Shay, P. A. Cassak, and W. H. Matthaeus

*Department of Physics & Astronomy, 217 Sharp Lab,
University of Delaware, Newark, Delaware 19716, USA*

(Dated: October 5, 2021)

Abstract

The kinetic evolution of the Orszag-Tang vortex is studied using collisionless hybrid simulations. In magnetohydrodynamics this configuration leads rapidly to broadband turbulence. At small scales, differences from magnetohydrodynamics arise, as energy dissipates into heat almost exclusively through the magnetic field. A key result is that protons are heated preferentially in the plane perpendicular to the mean magnetic field, creating a proton temperature anisotropy as is observed in the corona and solar wind.

The dissipation of turbulent energy in plasmas plays a critical role in understanding coronal heating and the acceleration of the solar wind [1], turbulence in the interplanetary medium [2], energy storage and release in the magnetosphere [3], and in a variety of other plasma and astrophysical contexts [4]. By “dissipation,” we mean the conversion of fluid scale energy irreversibly into kinetic degrees of freedom. A key observational clue about the nature of this dissipation is the substantial heating of protons, often preferentially in the plane perpendicular to the mean magnetic field[1, 5], both in the solar wind (plasma $\beta = (\text{thermal speed}/\text{Alfvén speed})^2 \sim 1$) and in the corona ($\beta \ll 1$). This heating has a variety of potential sources, including shocks and wave-particle interactions involving non thermal distributions such as pickup ions, but the ubiquity of broadband Kolmogoroff-like fluctuations suggests that kinetic absorption of fluid energy at or beyond the high wavenumber end of the inertial range plays an important role.

A fundamental demonstration of turbulent anisotropic heating is needed as a first step towards a basic physics understanding of the dissipation processes that heat the solar corona and solar wind. Magnetohydrodynamics (MHD) is a very useful plasma model which generally employs small but nonzero viscosity and/or resistivity, but this is not easily justified for collisionless systems where the mean free path is comparable to the system size (as in most of the corona and solar wind). More sophisticated attempts to numerically model plasma dissipation, e.g., by employing hyperresistivity, hyperviscosity or indirectly by including the Hall or finite Larmor radius effects (see [6]), include only selected approximations to kinetic effects, and therefore do not include the wider range of mechanisms available to the kinetic plasma.

In this paper, we report a demonstration of turbulent anisotropic proton heating in the Orszag-Tang vortex[7] using a hybrid simulation, which includes all proton kinetic effects. The hybrid simulation results are very similar at large length scales to MHD simulations of the same system, but show significant differences at small scales where kinetic effects are important. Analysis of the hybrid results show that energy is dissipated into proton heating almost exclusively through the magnetic field and not through the proton bulk velocity. The proton heating occurs preferentially in the plane perpendicular to the mean magnetic field. These simulations, to our knowledge, are the first self consistent demonstration of turbulent anisotropic proton heating. Finally, effective transport coefficients from the hybrid simulations are calculated, showing that the approximation of constant resistivity η is

potentially reasonable (although it cannot reproduce the proton temperature anisotropy), but a constant viscosity ν is untenable.

The Orszag-Tang vortex[7] is a well studied MHD initial configuration given by

$$\mathbf{B} = -\sin y \hat{\mathbf{x}} + \sin 2x \hat{\mathbf{y}} + B_g \hat{\mathbf{z}}; \quad \mathbf{v} = -\sin y \hat{\mathbf{x}} + \sin x \hat{\mathbf{y}} \quad (1)$$

with \mathbf{B} the magnetic field (B_g a uniform guide field) and \mathbf{v} the proton bulk velocity in normalized units described later. This configuration leads immediately to strong nonlinear couplings, producing cascade-like activity that might reasonably approximate the highest wavenumber decade of the inertial range. These couplings, which are dominantly local in wavenumber, in turn drive the dissipation range. The physics of the Orszag-Tang vortex has been previously studied using incompressible [7] and compressible [8] MHD simulations. Its robust production of nonlinear activity is a motivation for its frequent use in validating numerical schemes (see e.g. [9]).

Simulating kinetic dissipation is difficult and computationally expensive due to the requirement of treating a wide range of length scales. By choosing a computational domain with approximately one decade of scale in the MHD range and another in the kinetic range, we can study the conversion of strongly driven MHD fluctuations into kinetic motions. An antecedent of the present study compared global behavior of hybrid and Hall MHD simulations [10], but included a mean in-plane magnetic field while not adequately resolving the proton inertial length.

We use the hybrid code P3D [11] in 2.5D, which models protons as individual particles and electrons as a fluid and evolves

$$\frac{d\mathbf{x}_i}{dt} = \mathbf{v}_i; \quad \frac{d\mathbf{v}_i}{dt} = \frac{1}{\epsilon_H} (\mathbf{E}' + \mathbf{v}_i \times \mathbf{B}) \quad (2)$$

$$\frac{\partial \mathbf{B}'}{\partial t} = \nabla \times (\mathbf{v} \times \mathbf{B}) - \epsilon_H \nabla \times \left(\frac{\mathbf{J}}{n} \times \mathbf{B}' \right) \quad (3)$$

$$\mathbf{B}' = \left(1 - \frac{m_e}{m_i} \epsilon_H^2 \nabla^2 \right) \mathbf{B}, \quad \mathbf{E}' = \mathbf{B} \times \left(\mathbf{v} - \epsilon_H \frac{\mathbf{J}}{n} \right) \quad (4)$$

where $\mathbf{J} = \nabla \times \mathbf{B}$ is the current density, $\epsilon_H \equiv c/(L_0 \omega_{pi})$ is the normalized proton inertial length, m_e and m_i are the electron and proton masses, \mathbf{x}_i and \mathbf{v}_i are the positions and velocities of the individual protons, and \mathbf{v} is the proton bulk flow speed. Length is normalized to L_0 , velocities to $V_0 = B_0/(4\pi m n_0)^{1/2}$, time to $t_0 = L_0/V_0$, and temperature to $B_0^2/(4\pi n_0)$. The average density is n_0 , and B_0 is the root mean square in-plane magnetic field. The

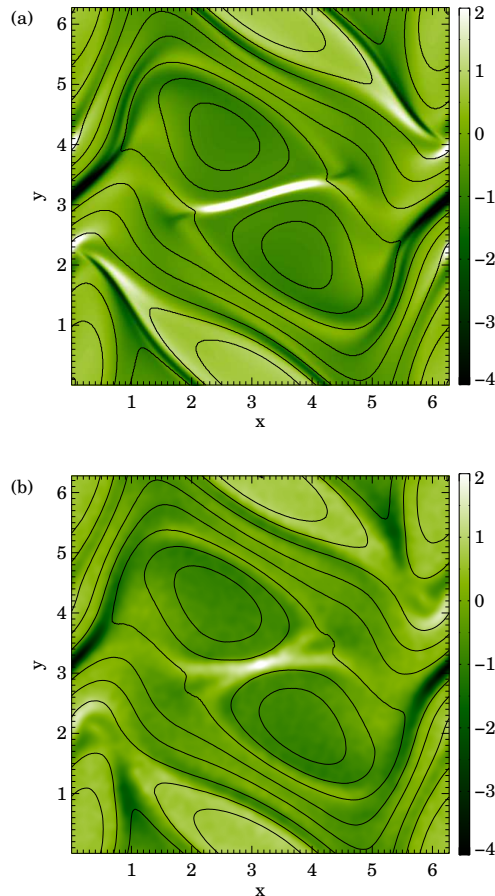


FIG. 1: (Color online) Current density with magnetic flux contours at $t=1.96$ in (a) fluid and (b) hybrid simulations.

magnetic field \mathbf{B} is determined from \mathbf{B}' using the multigrid method. The code assumes quasi-neutrality. The electron temperature is zero and is not updated.

Hybrid simulations are ideally suited for exploring dissipation and proton heating in collisionless plasmas because they include a complete kinetic description of protons. Due to the finite temperature of the protons, kinetic Alfvén waves are present in this set of hybrid simulations ([12, 13] and references therein), as well as parallel proton bulk flows.

The simulation domain is a square box of side length $2\pi \times 2\pi$ with 512×512 grid points. About 2.6 million protons are loaded with an initial Maxwellian distribution having a uniform temperature $= 8$, and $\epsilon_H = 2\pi/25.6$ and $m_e = 0.04m_i$. No artificial dissipation is present other than grid scale dissipation. Choosing a guide field $B_g = 5$ (total $\beta = 2nT/B^2 \approx 0.62$) reduces the system compressibility. Incompressibility is further promoted

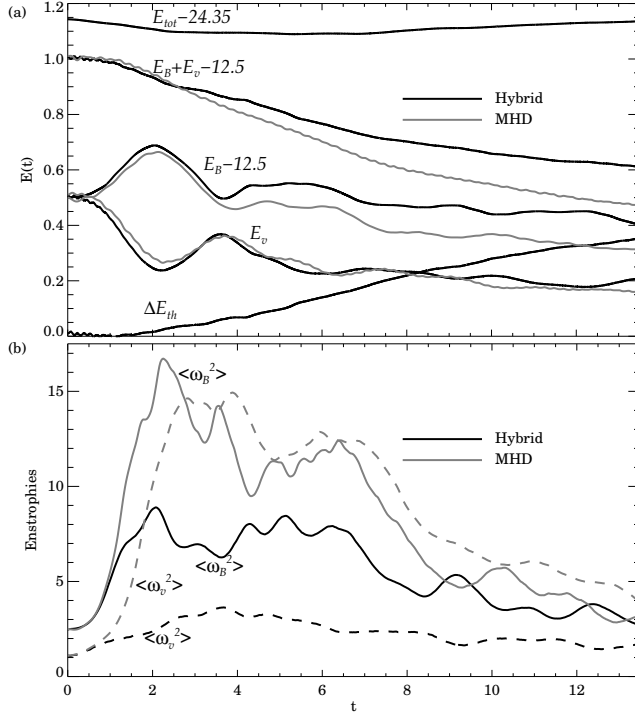


FIG. 2: Hybrid and MHD comparison: (a) Magnetic energy E_B , fluid flow energy E_v , their sum, the change in thermal energy ΔE_{th} , and total energy E_{tot} vs. time. (b) Flow enstrophy $\langle \omega_v^2 \rangle$ and magnetic enstrophy $\langle \omega_B^2 \rangle$ vs. time.

by adding perturbations to the background density n_0 that enforce $\partial(\nabla \cdot \mathbf{v})/\partial t = 0$ at $t = 0$. Simulations without the added perturbation show only small differences.

The hybrid simulation results are compared to those of a compressible 2.5 D MHD version of the code F3D [14] with constant and uniform resistivity $\eta = 0.0048$, zero viscosity ν , and ratio of specific heats $\gamma = 5/3$. (We motivate values for η and ν later.) In both cases, the magnetic islands initially centered on the midplane ($y = \pi$) begin a clockwise rotation. The initial velocity profile shears the magnetic islands until $t \sim 2$ as the islands approach and undergo a brief period of magnetic reconnection from $t \sim 2 - 4$. After $t \sim 4$, the system is dominated by strong turbulence. A comparison of out-of-plane current density J_z and magnetic field lines at $t = 1.96$ is shown in Fig. 1. The hybrid and MHD results show strong similarities at large scales, but significant differences at small scales where kinetic effects become important.

We can quantify the differences by comparing energy and dissipation budgets, where flow

energy $E_v = \langle \rho |\mathbf{v}^2|/2 \rangle$, magnetic energy $E_B = \langle |\mathbf{B}|^2/2 \rangle$, thermal energy E_{th} (total proton kinetic energy minus flow energy), and total energy E_{tot} . $\langle \dots \rangle$ denotes a volume average. Grid scale fluctuations in the hybrid data are smoothed using a standard local, weighted iterative averaging.

Figure 2(a) shows E_v, E_B , their sum, ΔE_{th} (where Δ means the change since $t = 0$) and E_{tot} , as a function of time from the hybrid and MHD simulations, with E_B and E_{tot} shifted down by a constant for convenience. Note that E_{tot} changes very little over the course of the hybrid run, demonstrating good numerical energy conservation. During the initial phase ($t < 2$), bulk flow energy is converted strongly into magnetic energy as field lines are stretched, but with little proton heating. The magnetic energy converts back to flow energy (with some heating) during the reconnection event ($t \sim 2 - 4$). Until $t \sim 4$, the energetics of the hybrid and MHD results are very similar. However, in the turbulent phase ($t > 4$), the hybrid and MHD codes show significant differences, and more dissipation occurs in the MHD case. Notably, the proton thermal energy increases monotonically during the turbulent phase in the hybrid simulation, even without explicit dissipation.

In MHD, mean square gradients of \mathbf{v} and \mathbf{B} are proportional to the energy dissipation rate. Although the hybrid code lacks explicit dissipation, it is instructive to compare in Fig. 2(b) the out-of-plane enstrophy (mean square vorticity) $\langle \omega_v^2 \rangle = \langle |\hat{\mathbf{z}} \cdot (\nabla \times \mathbf{v})|^2 \rangle$ and out-of-plane magnetic enstrophy (mean square current density) $\langle \omega_B^2 \rangle = \langle |\hat{\mathbf{z}} \cdot (\nabla \times \mathbf{B})|^2 \rangle = \langle J_z^2 \rangle$ in the hybrid and MHD simulations. At early time ($t < 4$), the hybrid and MHD enstrophies peak at about same time, but their magnitudes are very different, indicating that the length scales in the hybrid case are larger, probably due to finite Larmor radius effects. During the turbulent phase ($t > 4$), the enstrophies continue to be different but the magnetic enstrophies are surprisingly similar. This suggests that the kinetic dissipation may have some resemblance to a classical resistivity, which we revisit later. Note that the value of enstrophy in the hybrid case is necessarily sensitive to the averaging that defines the fluid scales.

To quantify the dissipation, consider the flow of magnetic energy in the system. Dotting the induction equation [Eq. (3)] with \mathbf{B} , averaging over space, and integrating over time gives

$$\Delta E_B(t) = - \int_0^t \langle \mathbf{v} \cdot (\mathbf{J} \times \mathbf{B}) \rangle dt' - \frac{d_e^2}{2} \langle \Delta J^2(t) \rangle - \mathcal{D}_B(t), \quad (5)$$

where Δ refers to the change since $t = 0$. The $\mathbf{v} \cdot (\mathbf{J} \times \mathbf{B})$ term, called ΔE_{vB} , is the exchange

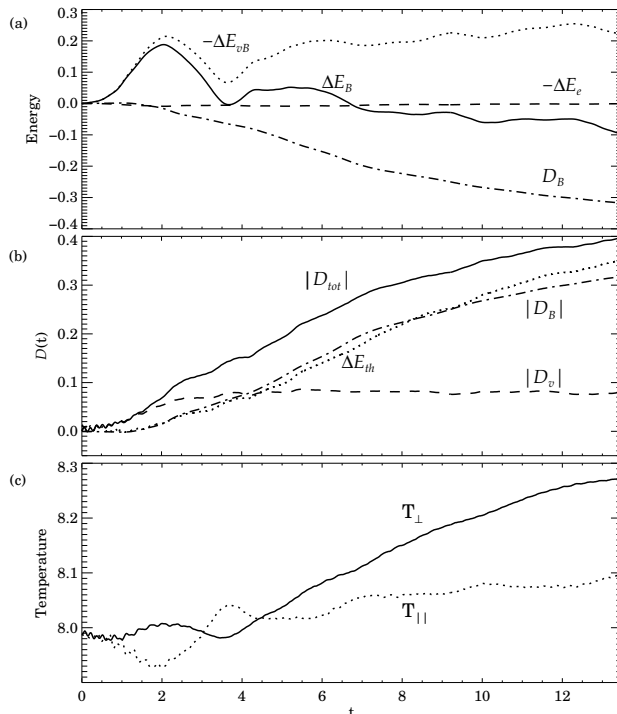


FIG. 3: (a) ΔE_B : change of E_B in the hybrid run; ΔE_{vB} : exchange between E_v and E_B ; ΔE_e : electron kinetic energy; \mathcal{D}_B : sum of these, total E_B dissipated. (b) \mathcal{D}_v and \mathcal{D}_B are cumulative dissipation through bulk flow and magnetic channels, \mathcal{D}_{tot} their sum, ΔE_{th} change in thermal energy. (c) Parallel and perpendicular proton temperatures vs. time.

in energy between bulk flow and the magnetic field and the d_e^2 term is essentially the electron kinetic energy. We define \mathcal{D}_B as the cumulative energy dissipated from the magnetic channel. Included in this term are non-MHD dissipative processes and grid scale dissipation. The first three terms are calculable from the simulations, so we may compute \mathcal{D}_B .

Fig. 3(a) shows that for $t < 4$, E_B increases due to input from E_v , then decreases as it is converted back. In the turbulent phase ($t > 4$), there continues to be conversion into magnetic energy. However, E_B decreases during this period, and both energy converted from the flow, and an approximately equal amount previously stored in the field, is absorbed in the magnetic dissipation \mathcal{D}_B .

A similar analysis can be done for energy flow in the bulk flow channel. Dotted the MHD momentum equation with \mathbf{v} and integrating over time and space gives

$$\Delta E_v(t) = \int_0^t \langle \mathbf{v} \cdot (\mathbf{J} \times \mathbf{B}) \rangle dt' - \mathcal{D}_v(t), \quad (6)$$

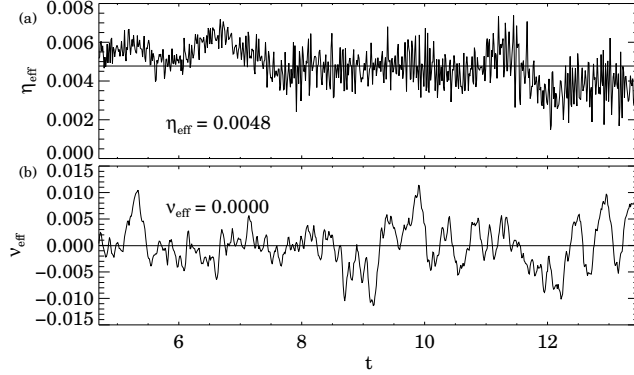


FIG. 4: Effective (a) resistivity η and (b) viscosity ν vs. time.

where \mathcal{D}_v is the cumulative energy converted into heat from the flow channel through non-fluid effects and compression. Fig. 3(b) shows \mathcal{D}_v (dashed line), \mathcal{D}_B (dot-dashed), $\mathcal{D}_{tot} = \mathcal{D}_B + \mathcal{D}_v$ (solid), and ΔE_{th} (dotted). In the turbulent phase ($t > 4$), there is essentially no energy dissipated through the flow channel (\mathcal{D}_v is constant). The energy dissipated through the magnetic field \mathcal{D}_B traces very closely the increase in thermal energy of the protons ΔE_{th} , so the main source of dissipation in this system is through magnetic interactions. The small departure between the two is accounted for by numerical heating, seen in the change in total energy E_{tot} [see Fig. 2(a)]; this is only about 10 % of the total dissipated magnetic energy

It is reasonable that little dissipation occurs through the flow channel. In the MHD regime (low wavenumber k), the dynamics of the hybrid simulation are at most weakly compressible, so the majority of energy is in oblique Alfvén waves that are weakly damped [15]. As energy cascades to smaller scales, the proton gyroradius is reached before the dissipation scale. Below the proton gyroradius, the ions decouple from the magnetic field and only weakly participate with the non-MHD waves in this region. Consequently, the Alfvén ratio E_v/E_B goes to zero in the kinetic regime as evidenced by the structure of kinetic Alfvén and whistler waves.

A central result of this study is that the dissipated magnetic energy preferentially heats the protons perpendicular to the mean magnetic field, as shown in Fig. 3(c). The perpendicular and parallel temperatures T_{\perp} and T_{\parallel} are calculated relative to the guide field. In the turbulent phase ($t > 4$), T_{\perp} increases monotonically, while T_{\parallel} remains relatively steady. The relative anisotropy is small because the available magnetic free energy in the system (from B_x and B_y) is small compared to the proton temperature, i.e. $\beta_{\perp} \gg 1$. If the heating

mechanism in this study generalizes to $\beta_{\perp} \sim 1$, large anisotropies will develop. The perpendicular heating occurs without any obvious connection to classical cyclotron resonances, as the latter generally are construed [16] to involve gyroresonance with waves propagating parallel to a background field (along the invariant direction in this study). Resonance can also involve wave frequencies near the cyclotron frequency; however, dominance in this simulation of incompressible modes and relatively low frequency kinetic Alfvén waves make the connection to standard cyclotron resonance [16] uncertain.

By assuming the classical functional forms for the dissipation rates $\eta\langle J_z^2 \rangle$ and $\nu\langle \omega_v^2 \rangle$, we can compute effective transport coefficients η_{eff} and ν_{eff} from the hybrid simulations. Figure 4 shows $\eta_{\text{eff}} = (\partial\mathcal{D}_B/\partial t)/\langle J_z^2 \rangle$ and $\nu_{\text{eff}} = (\partial\mathcal{D}_v/\partial t)/\langle \omega_v^2 \rangle$ versus time. Surprisingly, the spatially averaged η_{eff} is fairly constant in time, as is often assumed in MHD models. The mean value is $\eta_{\text{eff}} = 0.0048$, corresponding to a magnetic Reynolds number of $S_{\text{eff}} = 4\pi V_0 L/\eta_{\text{eff}} c^2 \approx 1308$, which is the value used in the MHD simulation. In classical turbulence theory, the length scale at which dissipation occurs λ_d is related to the Reynolds number and energy containing scale L through $S_{\text{eff}} \sim (L/\lambda_d)^{4/3}$ [17]. For the hybrid simulation, $\lambda_d \sim 0.029$, which is of the order of the electron skin depth, $c/\omega_{pe} \sim 0.049$. The spatially averaged ν_{eff} , on the other hand, shows oscillations much larger than the mean, calling into question the assumption of a non-zero viscosity assumed in many MHD models.

The effective resistivity being fairly constant does not imply that the dissipation is of the form ηJ^2 . The MHD simulations performed with this η_{eff} show more dissipation of B than the hybrid simulations, and cannot reproduce the preferential heating of T_{\perp} . Future studies will investigate the spatial dependence of η_{eff} , and its dependence on electron/proton inertial lengths, as well as system size. We will also examine the effect of reducing the guide field and including electron pressure in Ohm's law. The physical mechanism which converts magnetic energy into proton heat remains an open question and is under investigation. Potential explanations are wave-particle interactions such as Landau damping.

This work is supported by NSF ATM-0539995, NASA NNG05GM98G and NNX-08AI47G (Heliophysics Theory program), and NERSC. The authors thank S. Servidio, S.P. Gary, and B. N. Rogers for enlightening conversations.

[1] S. R. Cranmer, Space Sci. Rev. **101** 229–294 (2002).

- [2] C. W. Smith et al., *Astrophys. J.* **645**, L85-L88, (2006).
- [3] D. Sundkvist et al., *Phys. Rev. Lett.*, **99** 025004 (2007).
- [4] S. R. Spangler, *Astron. Astrophys.* **407**, 563 (2003).
- [5] C.-Y. Tu and E. Marsch, *Space Sci. Rev.* **73**, 1 (1995).
- [6] M. L. Goldstein et al., *Springer Lecture series in Physics* (1999).
- [7] S.A. Orszag and C.-M. Tang, *J. Fluid Mech.* **90**, 129 (1979).
- [8] R. B. Dahlburg and J. M. Picone, *Phys. Fluids B* **1**, 2153 (1989).
- [9] D. Rosenberg et al., *New J. Phys.* **9**, 304 (2007).
- [10] A. Matthews et al., *Lecture Notes in Physics* **462**, (1995).
- [11] M. A. Shay et al., *J. Geophys. Res.* **106**, 3715 (2001).
- [12] B. N. Rogers et al., *Phys. Rev. Lett.* **87**, 195004 (2001).
- [13] G. G. Howes et al., *Astrophys. J.* **651**, 590 (2006).
- [14] M. A. Shay et al., *Phys. Plasmas* **11**, 2199 (2004).
- [15] S. P. Gary, *J. Geophys. Res.* **104**, 6759 (1999).
- [16] P. A. Isenberg et al., *J. Geophys. Res.* **106**, 5649 (2001).
- [17] G. K. Batchelor, *The theory of homogeneous turbulence* (Cambridge University Press, Cambridge, 1953).